Quantitative Mass Spectrometry of Human Reticulocytes Reveal Proteome-wide Modifications During Maturation

Trang T.T. Chu[1¶], Ameya Sinha[1¶], Benoit Malleret[2,3], Rossarin Suwanarusk[3], Jung Eun Park[4], Renugah Naidu[1], Rupambika Das[1], Seow Theng Ong[5], Navin Kumar Verma[5], Jerry K. Chan[6,7], Francois Nosten[8,9], Laurent Rénia[3], Siu Kwan Sze[4], Bruce Russell[2,10] & Rajesh Chandramohanadas[1,6*]

[1] Pillar of Engineering Product Development (EPD), Singapore University of Technology & Design (SUTD), Singapore.
[2] Department of Microbiology & Immunology, Yong Loo Lin School of Medicine, National University of Singapore, Singapore.
[3] Singapore Immunology Network (SIgN), Agency for Science & Technology, Singapore.
[4] School of Biological Sciences, Nanyang Technological University, Singapore.
[5] Lee Kong Chian School of Medicine, Nanyang Technological University, Singapore.
[6] Department of Reproductive Medicine, KK Women's and Children's Hospital, Singapore.
[7] Duke-NUS Medical School, Singapore.
[8] Shoklo Malaria Research Unit, Mahidol-Oxford Tropical Medicine Research Unit, Faculty of Tropical Medicine, Mahidol University, Mae Sot Thailand.
[9] Centre for Tropical Medicine and Global Health, Nuffield Department of Medicine Research building, University of Oxford Old Road campus, Oxford, UK.
[10] Department of Microbiology and Immunology, Otago University, Dunedin, New Zealand.

[¶] These authors contributed equally to this work.

Running Title: Proteomics of Human Cord Blood-derived Reticulocytes

Corresponding Author: Rajesh Chandramohanadas

(rajesh@sutd.edu.sg)

Key words: Reticulocytes, Red blood cells, Quantitative Proteomics, iTRAQ, Atomic Force Microscopy, Cytoskeleton

Summary

Erythropoiesis is marked by progressive changes in morphological, biochemical and mechanical properties of erythroid precursors to generate red blood cells (RBC). The earliest enucleated forms derived in this process known as reticulocytes, are multi-lobular and spherical. As reticulocytes mature, they undergo a series of dynamic cytoskeletal re-arrangements and the expulsion of residual organelles, resulting in highly deformable biconcave RBCs (normocytes). To understand the significant, yet neglected proteome-wide changes associated with reticulocyte maturation, we undertook a quantitative proteomics approach. Immature reticulocytes (marked by the presence of surface transferrin receptor, CD71) and mature RBCs (devoid of CD71) were isolated from human cord blood using a magnetic separation procedure. After sub-fractionation into membrane and luminal samples, quantitative mass spectrometry (iTRAQ) was conducted to identify more than 1800 proteins with good confidence and coverage. While most structural proteins (such as Spectrins, Ankyrin and Band 3) as well as surface glycoproteins were conserved, proteins associated with microtubule structures, such as Talin-1/2 and ß-Tubulin were detected only in immature reticulocytes. Atomic force microscopy (AFM)-based imaging revealed extended network of spectrin filaments in reticulocytes (with an average length of 48 nm) which shortened during reticulocyte maturation (average spectrin length of 41 nm in normocytes). The extended nature of cytoskeletal network may partly account for increased deformability and shape changes, as reticulocytes transform to normocytes.

Introduction

Red blood cells (RBCs) mediate critical physiological functions such as cellular gaseous and nutrient exchange. They evolve from hematopoietic stem cells (HSCs) in bone marrow through a complex maturation cascade. HSCs first differentiate to form erythroid precursors called erythroblasts, before undergoing a series of divisions followed by extrusion of nuclei to derive reticulocytes [1-2]. The exact molecular process whereby multi-lobular, rigid reticulocytes mature into to the biconcave and highly deformable normocytes is poorly defined. A recent study by Malleret *et al* highlighted the need for further investigations into biochemical composition of maturing reticulocytes [3].

Reticulocyte maturation occurs through the loss of organelles via exocytosis, autophagy and re-arrangement of its cytoskeleton [2, 4-5]. Reticulocytes possess remnants of the translational machinery such as ribosomes, mitochondria, Golgi apparatus and lysosomes [6-7]. A significant number of surface membrane proteins are also lost in this transition [3]. Mature and immature forms of red cells are readily distinguishable microscopically due to visible morphological differences, however, the molecular mechanisms leading to their maturation remains largely unclear. Understanding protein dynamics during the final phases of erythropoiesis would shed light on pathological conditions whereby red blood cell maturation is impaired, for example reticulocytosis and related anaemia. Reticulocyte maturation also serves as an excellent model to understand vesicular trafficking since it involves organelle extrusion and degradation. Most of the previous attempts on profiling the human red blood cell proteome focused on either mature RBCs or reticulocytes derived from rodent models, which is quite dissimilar to human blood cells [6-8]. While a recent proteomic study [9] used human RBC blood cell populations (derived from *in vitro* cultures), this study like many others neglects the specific and synchronous differentiation between reticulocyte populations. In contrast, we purified immature reticulocytes positive for transferrin receptor (CD71) from human cord blood using a magnetic purification protocol [10] and conducted quantitative proteomics in comparison to late-stage retioculocytes and normocytes ($CD71^-$).

These enriched and purified samples were sub-fractionated to luminal and membrane components prior to quantitative mass spectrometry. The proteomic analyses identified a collective total of 1800 proteins with good confidence (FDR < 1%, and minimum 2 peptides identified). In this study we show the dynamics of red cell proteins between $CD71^{+}$ and $CD71^{-}$ RBCs and discuss how some of these key changes impact on the biological and bio-mechanical characteristics of reticulocyte maturation. Taken together, our work provides a valuable dataset linking bio-molecular and bio-mechanical characteristics along reticulocyte maturation.

Experimental Procedures

Blood collection and Ethics Statement

Cord blood samples used for mass spectrometry were collected from donors who who visited clinics under Shoklo Malaria Research Unit (SMRU), Mae Sot- Thailand as approved by the ethics committees of the Faculty of Tropical Medicine, Mahidol University, the Thai Ministry of Public Health, and the Institute for the Development of Human Research Protection and by the Oxford Tropical Research Ethics Committee (Ethical approval: OXTREC no.17-11). For validation studies, umbilical cord blood was collected from normal term pregnancies at KK Women's and Children's Hospital where women gave written informed consent for its use for this research.

Enrichment of reticulocytes by MACS purification

Selection of $CD71^+$ reticulocytes from cord blood was performed using the MACS purification system (Miltenyi Biotec, Singapore) [3,10]. Two mL of cord blood (from 5 independent donors) at 50% haematocrit in phosphate-buffered saline (PBS) was incubated with magnetic beads conjugated to CD71 antibody (Miltenyi Biotec) for 20 minutes at room temperature. After incubation, the blood sample was passed through a MACS LS column followed by three times washing with PBS. Flow through ($CD71^-$) and bound fractions ($CD71^+$) were collected and purity was monitored by flow cytometry using Thiazole orange staining and/or sub-vital staining. Samples were verified for purity (>90%) prior to MS analysis.

Sample fractionation for proteomic analysis

$CD71^+$ and $CD71^-$ red cells were sub-fractionated to membrane and luminal contents with slight modifications to a previously established protocol [11]. To do this, cells were washed thoroughly and lysed using 5 volumes of 0.02% saponin in PBS containing protease inhibitors (PI) on ice for 10 minutes. Un-disrupted cells, debris and magnetic beads were removed by sedimenting at 500×g for 10 minutes. The supernatant obtained was diluted in 20 volumes of ice-cold PBS and centrifuged at 50,000 rpm (approximately 170,000×g in Type 70Ti rotor, Optima™ L-100 XP

Ultracentrifuge, Beckman Coulter) for 3 h to sediment the membrane components. The membrane pellet obtained was washed at least twice with cold PBS/PI until it was cleared of haemoglobin. The pellet was extracted using 1% Triton X-100/PBS and precipitated with ice-cold acetone overnight. Simultaneously, supernatant fraction containing luminal contents were concentrated using 5kDa cut-off centrifugal filters (Amicon, Millipore). Protein concentration was estimated using a commercial BCA assay kit (Thermo Fisher Scientific). 40 µg of the supernatant (containing cytosolic somponents) and 20 µg of the membrane samples were resolved on 4-15% gradient Tris gel (Bio-Rad) and stained using colloidal coomassie (Sigma Aldrich G250).

Sample preparation and iTRAQ labeling for mass spectrometry

Luminal proteomic samples (200 µg each) were separated on 12% polyacrylamide gel by electrophoresis. In order to identify low abundant proteins in the samples, the extremely high abundant haemoglobin bands were discarded and the remaining gel slices were cut into small pieces. Further, gel pieces were de-stained with 25 mM triethylammonium bicarbonate (TEAB) in 50% acetonitrile (ACN) and dehydrated with 100% ACN. Samples were reduced in 5 mM Tris 2-carboxy-ethyl phosphine hydrochloride (TCEP) in 25 mM TEAB at 60°C for 45 min and alkylated in 55 mM iodoacetamide (IAA) in 25 mM TEAB for 1 h at room temperature in the dark. Following reduction/alkylation, gel pieces were further dehydrated with 100% ACN and digested in 25 mM TEAB containing 10 ng/ml sequencing grade modified trypsin (Promega, Madison, WT) at 37°C for 16 h.

Total 180 µg of membrane proteins from each sample were reduced directly in 5 mM TCEP for 3 h at 30°C and then alkylated in the dark using 55 mM IAA for 1h at room temperature. Reduced and alkylated proteins were subjected to in-solution trypsin digestion at 37°C for 16 h. Prior to iTRAQ labeling (AB Sciex, Singapore), the tryptic peptides extracted from soluble and membrane samples were desalted using a Sep-Pak C18 cartridge (Waters, Milford, MA) and dried in a vacuum concentrator. Dried peptides were labeled with the isobaric tags as followed: $CD71^-$ soluble sample was labeled with 114; $CD71^+$ soluble sample was labeled with 115; $CD71^-$ membrane sample was labeled with 116; $CD71^+$ membrane sample was labeled with 117 isobaric

tag. The labeled samples were combined and subsequently separated by high pH reversed-phase (HPRP) HPLC.

HPRP-HPLC fractionation and Mass Spectrometry analysis

The labelled peptides were fractionated using an X Bridge C18 column (Waters; 4.6 x 250 mm, 5-µm, 300Å) on a Prominence UFLC system (Shimadzu, Kyoto, Japan). Mobile phase A (0.02% NH_4OH) and mobile phase B (0.02% NH_4OH , 80% ACN) were used with a 60 min gradient of 5–10% B over 3 min, 10–35% B over 45 min, 35–70% B over 50 min followed by 55min at 100% B (constant flow rate of 1 ml/min). Sixty fractions were collected, concatenate combined into 20 pooled fractions, and then vacuum-dried for subsequent LC-MS/MS analysis. LC-MS/MS analyses were performed on the iTRAQ labelled sample using a Ultimate 3000 RSLC nano-HPLC system (Dionex, Amsterdam, NL) coupled to a QExactive Hybrid Quadrupole-Orbitrap Mass Spectrometer (Thermo Scientific Inc., Bremen, Germany). The LC-MS/MS analysis was performed in triplicate by injecting the samples three times. The mass spectrometer was set to perform data acquisition in the positive ion mode with a selected mass range of 350–1600 m/z. Peptides with 2+ to 4+ charge states were selected for MS/MS. The ten most abundant peptides above a 1000 threshold were selected for MS/MS with a 2Da isolation width and dynamically excluded for 30 s.

Data Analysis

Protein identification and peptide quantitation were performed by querying against Uniprot Human database (Released on 11/29/2013; 176,946 sequences, 70,141,034 residues) complemented with its reverse sequence for false discovery rate determination by means of an in-house Mascot server (version 2.4.1, Matrix Science, London, UK). Defined parameters were as follows: (i) iTRAQ 4-plex (ii) cysteine carbamidomethylation was set as fixed modification whereas methionine oxidation and asparagine deamidation were set as variable modification (iii) trypsin digestion with maximum two missed cleavage (iv) peptide precursor mass tolerances of 10 ppm (v) mass tolerance of 0.02 Da for fragment ions. The mascot results were exported as csv files for further analysis in Excel program. The following parametes were used by

Mascot for protein quantification: outliners: auto; normalization: none and only unique peptides of the protein were used for iTRAQ quantification.

Ingenuity (Qiagen) and Cytoscape (ClueGo plugin) were used to annotate the proteins and perform a pathway analysis between the reticulocyte and normocyte fractions. Broadly, the genes were annotated in to three categories – (1) biological process, (2) subcellular localization and (3) molecular function. Their gene ontology under each of these categories was obtained by querying the UniProt accession numbers against the Gene Ontology database with Cytoscape plugin ClueGO. We defined up-regulated and down-regulated (as an indication of abundance and reduction in relative protein amounts, as the reticulocytes mature) at an arbitrary threshold for proteins showing at least a 2-fold difference between samples with a standard deviation of less than 20%. Ingenuity (Qiagen) maintains a database that ascertains which proteins are enriched in a well-defined pathway compared to a background reference. It provides a corresponding *p* value, which reflects the statistical significance of the pathways ascertained.

Experimental Design and Rationale

The human cord blood samples used in this study to isolate red cell sub-populations were derived from 5 adults, minimizing intrinsic variability between individuals. For comparative analysis between young and immature erythroid cells, internal controls were included (proteins known to be consistent in level, e.g. α-globin, flotillin, stomatin between these cells). For all the changes identified and reported herein, robust analysis and validation using additional samples and complementary techniques were performed. Only proteins that fell within < 1 % FDR threshold were included for various analysis.

Western Blotting and Immunofluorescence Microscopy

Mass spectrometry results were validated by Western immunoblotting and immunofluorescence confocal microscopy. For Western blotting, representative protein samples were resolved on 10 % SDS-PAGE, transferred to PVDF membrane (Amersham, GE Healthcare Life Sciences) using a semi-dry blot apparatus (Bio-rad)

and probed with appropriate primary antibody in 5% (w/v) non-fat dry milk in PBS overnight in the following dilutions: mouse monoclonal anti-Talin (1:2000, Abcam), rabbit polyclonal anti-β-tubulin (1:1000, Abcam), rabbit polyclonal anti-α-adducin (1:2000, Abcam), mouse monoclonal anti-spectrin (1:5000, Abcam), mouse monoclonal anti-band 4.1 (1:1000, Sigma), rabbit polyclonal anti-actin (1:1000, Sigma), mouse monoclonal anti-flotillin 1 (1:1000, BD), rabbit monoclonal anti-α-Fodrin (1:1000, Abcam), and mouse monoclonal anti-CD71 (1:1000, BD Biosciences). Next, appropriate HRP-conjugated secondary antibody (GE Healthcare Life Science) was incubated at 1:10,000 for 1 h at room temperature. The immunoblots were developed using an enhanced chemiluminescene detection kit (ECL, Amersham GE Healthcare Life Sciences).

For confocal microscopy, cells were attached to poly-L-lysine-coated coverslips before fixing with 4% (v/v) formaldehyde and then permeabilized with 0.03% (v/v) Triton X-100 in blocking buffer (3% BSA (w/v) in PBS). After blocking, cells were incubated with primary antibodies (anti-CD71, anti-β-Tubulin, anti-Talin-1 or anti-Band3) for 1 h followed by fluorescently labelled secondary antibodies. CellMaskTM Orange (Thermo Fisher Scientific) was used to visualize the cell membrane and Thiazole Orange was used as a marker for reticulocytes when staining the cord blood samples. Fluorescence confocal images were acquired by a Zeiss LSM 800 Airyscan Microscope (Carl Zeiss Microimaging Inc., NY, USA) equipped with 405-, 488-, 561- and 640-nm excitation lasers using a Plan-Apochromat 63× / 1.4 Oil DIC M27 objective lens (Carl Zeiss) as described [12]. Laser percentage and digital gain for each laser channels were kept identical for visualising various samples and the images were processed using Zen 2.1 lite imaging software (Carl Zeiss) keeping similar settings for each sample groups.

Atomic Force Microscopy

Cytoplasmic-surface-exposed samples used for cytoskeletal imaging were prepared as described previously [13-15]. Imaging was performed with a JPK Nanowizard II AFM instrument (JPK Instrument AG, Germany) using super sharp silicon probes (SSS-NCHR probes, Nanosensor, Neuchatel, Switzerland) in intermittent air contact

mode. Height images were captured at a resolution of 512 × 512 pixels for 1 μm × 1 μm areas with 0.5 Hz scan rate. NanoWizard image processing software (JPK Instruments AG) was used to generate images with sample height profiles. Images were smoothed using a low-pass filter based on Gaussian convolution kernel, resulting into topographical height images of sample surface. ImageJ was used for end-to-end spectrin length measurements. For improved accuracy, several hundreds of mesh loops were manually measured using freehand tool in ImageJ. To quantify the cytoskeletal mesh size, we used Matlab (R2013b) and built skeletonized images from coordinate matrix (withdrawn from JPK data software) and evaluated the average mesh size of each skeletonized image as reported previously. One-way ANOVA was used to confirm significance.

Micropipette Aspiration

A borosilicate glass micropipette was used to extract the RBC membrane shear modulus through micropipette aspiration method [14]. Pipettes were drawn from borosilicate glass tubing (Sutter Instrument Model P-2000) and cut open (Narishige MF-900) before mounting to the micromanipulator for measurements. The micropipette's inner diameter was maintained at approximately 2 ± 0.5 μm for all measurements. A pressure drop rate of 1 Pa/s and a total pressure drop of 100 Pa were applied in order to aspirate and deform each cell during measurement. A sample size of at least 20 cells/sample was taken for individual experiments. The cell membrane was monitored by Olympus I × 71 microscope and processed by QCapture™ Pro 6.0 as described in prior work. From the high-resolution recordings, the leading edge of the aspired RBC membrane was tracked manually for calculating the elastic shear modulus using the Hochmuth model [16]. Images were anlyzed and plotted using Graph Pad prism, Two-tailed t-test were performed to determne statistical significance.

Results

Isolation of Reticulocyte sub-populations from Human Cord Blood

Until recently, it was difficult to study the various stages of reticulocyte sub-populations, except for noting gross morphology and sub-vital staining patterns using the Heilmeyer stage classification. Attempts to separate the various reticulocyte stages using Percoll density gradients, often resulted in low yield and purity [17]. Using a more recent method optimized by Malleret *et al* [3], it is possible to select the immature reticulocytes (Heilmeyer class I through III) from the cord blood by magnet assisted cell sorting (MACS). In this method, magnetic beads coupled to CD71 antibody are used to selectively enrich cells that are positive for transferrin receptor ($CD71^+$). Cells that are part of the flow-through include mature reticulocytes and normocytes, both of which lack CD71. A schematic representation of the procedure for reticulocyte enrichment and sample processing is illustrated as **Scheme. 1**. Upon collecting the samples by centrifugation, homogeneity of the cells purified was tested by Thiazole Orange staining and flow cytometry. **Figure. 1A** shows the flow cytometry profiles corresponding to $CD71^+$ (Upper Panel) and $CD71^-$ (Lower Panel) RBCs isolated by MACS, confirming efficient separation of cells. A small positive population (4.1%) visible for $CD71^-$ cells are indicative of a transforming reticulocyte population (Heilmeyer class IV). Sample smears (**Figure. 1B**) stained with methylene blue shows a reticular staining pattern indicative of residual RNA present only in the $CD71^+$ population. Differential interference contrast (DIC) microscopy (**Figure. 1B**) clearly showed distinct morphological characteristics of the two cell types. While the $CD71^-$ RBCs showed characteristic biconcave shape, the $CD71^+$ RBCs had multiple lobes, unique for early-stage reticulocytes. In addition, we probed these samples using a different CD71 antibody via immunofluorescence microscopy (**Figure. 1C**) and Western blotting (**Figure. 1D**) to confirm efficient separation of $CD71^+$ reticulocytes from those negative for CD71. Overall, these results confirm high degree of purity of the samples used for mass spectrometric experiments.

Sample Preparation and Mass Spectrometry

To reduce sample complexity (thereby allowing detection of maximum number of proteins), we separated each sample into membrane and luminal sub-fractions after

lysing the cells using low concentrations of saponin (0.02% in PBS) followed by separation by ultracentrifugation. This has been previously adopted for proteomic studies involving malaria parasite-infected red blood cells [11, 18]. Details of sample preparation and procedures are provided in the methods section. After fractionation, representative samples from membrane and luminal sub-fractions were resolved on a 4-10% SDS-PAGE (**Figure. 1E**). Samples corresponding to the membrane proteome showed enrichment of components such as spectrins (~ 250kDa) and band 3 (90-100kDa), at the expected molecular weight regions. Both soluble and membrane sub-fractions derived from $CD71^+$ reticulocytes appeared more complex in overall protein profile, compared to corresponding material from $CD71^-$ erythrocytes. In the soluble fraction, multiple high MW proteins were present, which most likely represented proteins from Golgi apparatus or Endoplasmic Reticulum (ER). High apparent molecular weight proteins may also indicate ubiquitinated proteins destined for targeted destruction. Almost 90% of the proteome for both samples was composed of haemoglobin, which appeared as a thick band in the 10-14kDa region of the SDS-PAGE gel. Haemoglobin signal from the membrane fraction was very low indicating high membrane sample purity and robust fractionation method. After ensuring sample purity, representative samples (~180 µg in total) were used for mass spectrometric analysis as described in the methods section. The iTRAQ LC-MS/MS data and the Mascot search results are deposited in the Proteome Xchange Consortium [19] via the PRIDE partner repository with the identifier PXD003851 (Supplemental Dataset S1).

Submission details (for review purpose only):

Project Name: Reticulocytes vs mature red blood cell

Project accession: PXD003851

Reviewer account details:

Username: reviewer25260@ebi.ac.uk

Password: wwtcEhDi

Protein Annotation and Data Curation

From the mass spectrometric analyses, a total of 1892 proteins were identified with a false discovery rate (FDR) of < 1% (**Supplemental Dataset 1**). A noteworthy

observation was that in a lysate where haemoglobin alone constitutes approximately 90% of the total proteins, the residual 10% of the proteome was made of an astonishing collection of gene products. However, the extent to which these molecules are biologically active or simply remnants from their erythroblast precursors is arguable. It should be highlighted that despite the extensive purification protocols and stringent identification criteria, the nature of the study is bound to include some false positives or contaminating proteins incorrectly associated with the red blood cell proteome. However, blood group antigens, like Kell (P23276), which are present in relatively low abundance were identified in all of the fractions denoting specificity of the sample preparation. In addition, hallmarks of standard contamination such as CD45 (P08575) which is a leukocyte surface antigen and GlycoproteinIIb/IIIa (P08514/P05106) an integrin complex present on platelets were not identified in our dataset, further confirming high sample purity.

Analysis of Membrane and Soluble Proteome

Figure. 2A depicts an Ingenuity Pathway Analysis (IPA) which defines relevance of proteins in canonical biological pathways by taking into account their expression values as a way to define relative abundance. Most of them are pertinent while considering the processes whereby the reticulocyte matures into a normocyte. Components of the eukaryotic initiation factor (EIF2) signalling pathway and its corresponding regulation are enriched in the reticulocyte. This represents primarily the translational machinery, which still may be active in immature reticulocytes. It also corresponds well with the gene ontology data indicating that majority of the proteins are ribosomal-associated. Interestingly, proteins associated with the ubiquitination pathway were abundant in $CD71^{+}$ reticulocytes, reflecting a mechanism of organelle degradation during reticulocyte maturation. It has already been shown that β-tubulin, aquaporin 1 (AQP1) and AP-2 utilize the proteosomal machinery to expunge themselves from the reticulocyte [20-21]. The oxidative phosphorylation pathway could be indicative of the passive signalling cascades which go on to phosphorylate cytoskeletal proteins and thus induce a conformational and/or morphological and biomechanical change in the reticulocyte as they develop. The phosphorylation status of band 3 affects the interaction between the membrane and

cytoskeleton of the RBC. Recent literature provides a strong link between a change in phosphoproteome of the cytoskeleton and integral membrane is the most likely cause of change in deformability [22-25].

To determine protein dynamics and patterns from the dataset, identified hits annotated to a particular term in the human GO slim (http://geneontology.org) ontology were used to construct various graphical representations shown in **Figure. 2**. Note that because genes can be categorized into more than one classification, there are more functional annotations than total number of genes with annotations. The gene ontology of the proteins (906) enriched in the membrane fraction of reticulocytes reflects that they belong to organellar membranes comprising of the translational and metabolic machinery- the ribosomes and mitochondria respectively (**Figure. 2B and 2C**).

The gene ontology of the luminal proteome, where 213 proteins were enriched, was the most complex of them all. There are diverse groups of proteins in this fraction belonging to various cellular processes (**Figure. 3A**) and sub-cellular locations (**Figure. 3B**); indicative of a typical cell since all the remnant enzymes and machinery still exists in early reticulocytes. The cellular localization ontology pattern confirms that our fractionation was good since the proteins that showed up in this sample set were almost all cytosolic. 169 proteins were reduced in the reticulocyte over the normocyte as part of this dataset (**Figure. 4A and 4B**). Of note, some of these proteins do not belong to cytosol despite the identification, yet, detected due to their relative abundance in the red cell. This is why their relative abundance and contribution to the entire gene ontology provides for some errors whereby most proteins belong to the polymerised actin and endosomal compartments.

Cytoskeletal Modifications during Reticulocyte Maturation

Analysis of our dataset revealed that majority of surface exposed proteins remained similar between the two red cell stages, including glycophorins, complement receptor 1 and band 3 anion exchange protein (**Figure. 5A**). Similarly, well-known membrane structural components including cytoskeletal proteins were identified and annotated

from the mass spectrometry data (**Figure. 5B**). A closer look, based on fold-change, confirmed relatively similar abundance for most of the major membrane and cytoskeletal components. Spectrins, ankyrin, band 3, band 4.1 and band 4.2, etc. were slightly higher in the fraction derived from $CD71^-$ cells in agreement with previous literature [5]. However, this could be attributed to reduced protein complexity and diversity in mature red cells compared to reticulocytes.

Of special note, we noticed remarkable abundance of β-tubulin (**Supplemental Figure. S1**) and talin-1/2 proteins (**Supplemental Figure. S2**) in $CD71^+$ cells and their loss upon maturation (**Figure. 5B**). These proteins are normally associated with microtubule structures and render adhesive [26] and mechanical properties [4, 27] to eukaryotic cells. Using Western immunoblotting (**Figure. 5C**), we were able to validate the loss of talin-1/2 and β-tubulin in mature red cells. To visualize the localization of both of these proteins, super-resolution immunofluorescence microscopy was carried out with anti-band 3 as a control for microscopy, which stained all cells from both $CD71^+$ and $CD71^-$ populations. (**Supplemental Figure. S3**). We detected strong fluorescence signals for both β-tubulin and talin-1 in $CD71^+$ cells, which were absent in $CD71^-$ normocytes (**Figure. 6A and 6B**). Notably, these proteins appeared neither assembled as a network of microtubules nor physically linked to the cell membrane, but as discrete punctate spots within the cytoplasm.

Next, we investigated how *ex vivo* maturation of $CD71^+$ reticulocytes impacts morphological and membrane bio-mechanical properties. To do this, reticulocytes enriched from cord blood by MACS purification were allowed to mature at 37^o C for 40 h. Cells were collected fresh (T0), 20 hours (T20) and 40 hours (T40) later for morphological and biomechanical property measurements. Clearly, the multi-lobular and stiff reticulocytes that were freshly isolated from cord blood (with an average membrane shear modulus of 18.9 pN/μm) were transformed to more deformable red cells (membrane shear modulus of 6.6 pN/μm) over 40 h (**Figure. 7A**), through expulsion of reticular matter. We also detected talin-1/2 and β-tubulin in supernatants collected from *ex vivo* maturation assays (data not shown), while $CD71^-$ cells remained the same (~5.4 pN/μm) throughout the period of incubation. However, loss

of talin-1/2 and β-tubulin is unlikely to explain changes in the biomechanical properties, since they were not part of the membrane/cytoskeleton in the first place, as observed from confocal microscopy.

Quantitative proteomics data showed no significant differences in the overall abundance of major structural proteins (e.g. spectrins and ankyrin) that form the core red cell structure. Therefore, we evaluated potential differences in the nano-structural arrangement of spectrin-based cytoskeleton, in an attempt to corroborate observed membrane property changes. For this, we employed Atomic Force Microscopy (AFM) analysis [13-15] on cytoplasmic surface-exposed reticulocytes and normocytes. Samples on functionalised coverslips were subjected to shear-washing followed by AFM imaging. Skeletonized images (**Figure. 7B**) were generated and used to estimate spectrin length for each cell type. A total of 743 measurements were conducted for end-to-end spectrin cross-members length. We observed that the spectrin length for reticulocyte sample was 48± 14.65 nm. Significant contraction in spectrin network was observed in mature RBCs (**Figure. 7C**) with average spectrin length reduced to 41 ± 9.58 nm, with little difference in terms of individual mesh size between two populations. Such contractions in skeletal networks could contribute to unique mechanical characteristics of reticulocytes, which requires further mechanistic investigations beyond the scope of this study.

Discussion

Mammalian erythrocytes have been subjects for extensive research, due to their functional relevance and associated disease states, such as sickle cell anaemia, thalassemia and malaria. However, very little is known about protein diversity and dynamics in young reticulocytes as they undergo maturation. Prior studies in this direction mostly used mouse blood for proteomic studies, which is quite dissimilar in protein composition compared to human RBCs [8]. A study that focused on reticulocytes used blood drawn directly from phenylhydrazine-administered mice, with reticulocyte counts not greater than 50% [6]. Bell *et al* [7], on the other hand, leveraged on *in vitro* cultured human HSCs, however, with a focus on early erythropoiesis while the erythroblasts develop into reticulocytes by nuclear extrusion. Combining Multiplex Tandem Mass Tag labelling with nanoLC-MS/MS, Wilson *et al* recently documented nearly 1600 proteins, while comparing adult and cord RBCs and reticulocytes [28]. This study by far is the most comprehensive in the context of red cell maturation. However, these analyses used *ex vivo* maturation of $CD34^{+}$ cells to derive reticulocytes, which results in non-synchronous population of reticulocytes, normoblasts and erythroblasts.

Our MS analyses of pure and synchronus reticulocyte populations identified more than 1800 proteins with good coverage and confidence, under robust conditions of stringency (<1% FDR, at least 2 unique peptides). Pre-fractionation of samples into membrane and luminal components allowed us to quantitatively look at remodelling events while the reticulocytes transition into normocytes. Our analyses revealed that luminal fraction of the immature reticulocytes, more or less, resembled a typical metabolically and translationally active mammalian cell, with proteins that belong to ribosomes, ER and Golgi apparatus. Vesicular components Alix (PDC6I), IST1 homolog (IST1), Vacuolar protein sorting-associated protein (VPS4A), Tumor susceptibility gene 101 protein (Q99816), Charged multi-vesicular body protein 4b (Q9H444) which are involved in expelling organelles out during the maturation process are abundant in reticulocytes. MHC Class I molecules (GO: 0002479) – beta-2-microglobulin (H0YLF3), HLA-B (B0UX83), HLA-A (P16188, P01892, P05534) showed a reduction in normocytes confirming a previous similar observation in mice

[29]. This would explain part of the transferrin-recycling scheme. There is evidence to support AP-2 involvement in the clathrin-mediated endocytosis of transferrin [21]. In addition, Dynamin-2 and Cortactin, both of which were also enriched substantiate literature, which shows their activation as the commencement of endocytosis [30]. An established model for cargo trafficking involves the conversion of early endosomes marked by RAB5 to late endosomes that contains RAB7. In addition, β-tubulin is the main constituent of microtubules in cells and are involved in trafficking endosomes [2]. Our data corroborates that these proteins are progressively lost upon reticulocyte maturation.

While Wilson *et al* [28] suggested an increase in the relative abundance of Ankyrin, Band-3 and 4.1R junctional complex, our mass spectrometry results are in agreement with Liu *et al* indicating little or no difference in these cytoskeleton proteins [4]. Our results also agree with Liu *et al* regarding the expression of peripheral membrane proteins such as Glycophorin A and Glycophorin C, as they do not undergo changes during reticulocyte maturation. The spectrin-based network tethering other cytoskeletal proteins such as ankyrin, protein 4.1 and actin to the predominantly viscous lipid bilayer is a critical contributor of red cell integrity and deformability dynamics [31]. Progressive alteration to the spectrin-based network due to a number of factors, including infection by malaria parasites, has been shown to cause changes in RBC deformability properties [13, 15]. We did not observe any significant differences in abundance of spectrin or other accessory proteins linked to spectrin that collectively derive the cellular architecture. Despite the remarkable morphological and bio-mechanical differences between $CD71^{+}$ and $CD71^{-}$ red cells, all these proteins remained unchanged.

Microtubule networks are part of the cytoskeletal organization in a typical cell and play important roles in cellular processes such as arrangement and compartmentalization of organelles providing structural integrity [27, 32], facilitating intracellular transport and more. Our proteomic data revealed that two proteins: β-tubulin and talin usually associated with microtubule structures, are present in high amounts in reticulocytes. While Konstantinidis and colleagues [27] illustrated the

requirement for tubulin polymerization for enucleation in erythroblasts, there is no other precedence towards depicting a biological role for tubulins in reticulocytes. Similarly, talin-1/2 in RBCs are known to be associated with actin filament assembly during adhesion [33]. In our microscopic validation experiments, both these proteins, however, were found scattered in the cytosol with no apparent physical contacts with the membrane proper. While it is likely that tubulin and talin present in reticulocytes are mere remnants (that remained from the precursor stage) with no apparent function, due to the versatile nature of cytoskeletal proteins in eukaryotic cells, plausible undiscovered roles in reticulocytes cannot be fully ruled out.

In blood cell disorders such as spherocytosis, thalassemia or sickle cell anemia, reduction in the surface area: volume occurs resulting in less deformable phenotypes [34-35]. The spectrin-based network beneath the cell membrane contributes largely to the shear elastic properties of the RBCs. It has been shown in prior work that reduction in the length of spectrin monomers within the spectrin network can lead to increased deformability and filterability [14-15] of the cell. Therefore, we chose to image the nano-strauctural arrangement of spectrin-based skeleton in $CD71^{+}$ and $CD71^{-}$ cell populations. In agreement with the anticipated results, we observed significant shrinkage in the spectrin filaments in normocytes compared to immature reticulocytes, which could partly explain the biophysical changes observed during reticulocyte maturation process.

Taken together, our data provides a detailed proteomic and biomechanical profile of the differences that exist between reticulocytes and normocytes. While linking up the differences in morphology and rigidity to human disease states, such as susceptibility preferential invasion of reticulocytes by human malaria parasites [36-37] require further targeted investigations, our data form an avenue to explore and formulate a starting hypothesis.

References

1. Dzierzak, E., and Philipsen, S. (2013) *Erythropoiesis: development and differentiation. Cold Spring Harb Perspect Med*. **3**(4): p. a011601.
2. Blanc, L., and Vidal, M. (2010) *Reticulocyte membrane remodeling: contribution of the exosome pathway. Curr Opin Hematol*. **17**(3): p. 177-83.
3. Malleret, B., Xu, F., Mohandas, N., Suwanarusk, R., Chu, C., Leite, J. A., Low, K., Turner, C., Sriprawat, K., Zhang, R., Bertrand, O., Colin, Y., Costa, F. T., Ong, C. N., Ng, M. L., Lim, C. T., Nosten, F., Rénia, L., and Russell, B. (2013) *Significant biochemical, biophysical and metabolic diversity in circulating human cord blood reticulocytes. PLoS One* **8**(10): p. e76062.
4. Liu, J., Guo, X., Mohandas, N., Chasis, J. A., and An, X. (2010) *Membrane remodeling during reticulocyte maturation. Blood* **115**(10): p. 2021-7.
5. Griffiths, R. E., Kupzig, S., Cogan, N., Mankelow, T. J., Betin, V.M., Trakarnsanga, K., Massey, E. J., Lane, J. D., Parsons, S. F., and Anstee, D. J. (2012) Maturing reticulocytes internalize plasma membrane in glycophorin A-containing vesicles that fuse with autophagosomes before exocytosis. *Blood* **119**(26):6296-30.
6. Prenni, J. E., Vidal, M., and Olver, C. S. (2012) Preliminary characterization of the murine membrane reticulocyte proteome. *Blood Cells Mol Dis.* **15**; 49 (2): 74-82.
7. Bell, A. J., Satchwell, T. J., Heesom, K. J., Hawley, B. R., Kupzig, S., Hazell, M., Mushens, R., Herman, A., and Toye, A. M. (2013). Protein Distribution during human erythroblast enucleation *in vitro*. *PLoS ONE*, **8**(4), e60300.
8. Pasini, E. M., Kirkegaard, M., Salerno, D., Mortensen, P., Mann, M., and Thomas, A.W. (2008) *Deep coverage mouse red blood cell proteome: a first comparison with the human red blood cell. Mol Cell Proteomics* **7**(7): p. 1317-30.
9. Gautier, E. F., Ducamp, S., Leduc, M., Salnot, V., Guillonneau, F., Dussiot, M., Hale, J., Giarratana, M. C., Raimbault, A., Douay, L., Lacombe, C., Mohandas, N., Verdier, F., Zermati, Y., and Mayeux, P. (2016) Comprehensive Proteomic Analysis of Human Erythropoiesis. *Cell Rep*. Aug 2;16(5):1470-84.

10. Malleret, B., Li, A., Zhang, R., Tan, K. S., Suwanarusk, R., Claser, C., Cho, J. S., Koh, E. G., Chu, C. S., Pukrittayakamee, S., Ng, M. L., Ginhoux, F., Ng, L. G., Lim, C. T., Nosten, F., Snounou, G., Rénia, L., and Russell, B. (2015) *Plasmodium vivax: restricted tropism and rapid remodeling of CD71-positive reticulocytes. Blood*, **125**(8): p. 1314-24.
11. Millholland, M. G., Chandramohanadas, R., Pizzarro, A., Wehr, A., Shi, H., Darling, C., Lim, C. T., and Greenbaum DC. (2011) *The malaria parasite progressively dismantles the host erythrocyte cytoskeleton for efficient egress. Mol Cell Proteomics*, **10**(12): p. M111 010678.
12. Fazil, M. H., Ong, S. T., Chalasani, M. L., Low, J. H., Kizhakeyil, A., Mamidi, A., Lim, C. F., Wright, G. D., Lakshminarayanan, R., Kelleher, D., and Verma, N. K. (2016) GapmeR cellular internalization by macropinocytosis induces sequence-specific gene silencing in human primary T-cells. *Sci. Rep.* 6, 37721.
13. Shi, H., Liu, Z., Li, A., Yin, J., Chong, A. G., Tan, K. S., Zhang, Y., and Lim, C. T. (2013) Life cycle-dependent cytoskeletal modifications in Plasmodium falciparum infected erythrocytes. *PLoS One* 8, e61170.
14. Sinha, A., Chu, T. T., Dao, M., and Chandramohanadas, R. (2015) Single-cell evaluation of red blood cell bio-mechanical and nano-structural alterations upon chemically induced oxidative stress. *Sci Rep* 5, 9768.
15. Dearnley, M., Chu, T., Zhang, Y., Looker, O., Huang, C., Klonis, N., Yeoman, J., Kenny, S., Arora, M., Osborne, J. M., Chandramohanadas, R., Zhang, S., Dixon, M. W., and Tilley, L. (2016) Reversible host cell remodeling underpins deformability changes in malaria parasite sexual blood stages. *Proc Natl Acad Sci U S A* **113**, 4800-4805.
16. Hochmuth, R. M. (2000) Micropipette aspiration of living cells. *J Biomech* **33**, 15-22.
17. Pawar, V. B., and Prabhu, A. (1991) Isolation of large numbers of fully viable human reticulocytes using continuous Percoll density gradient. *Clin Lab Sci*,. **4**(6): p. 360-4.
18. Chandramohanadas, R., Davis, P. H., Beiting, D. P., Harbut, M. B., Darling, C., Velmourougane, G., Lee, M. Y., Greer, P. A., Roos, D. S., and

Greenbaum, D. C. (2009) Apicomplexan parasites co-opt host calpains to facilitate their escape from infected cells. *Science*, **324**(5928): p. 794-7.

19. Vizcaíno, J. A., Deutsch, E. W., Wang, R., Csordas, A., Reisinger, F., Ríos, D., Dianes, J. A., Sun, Z., Farrah, T., Bandeira, N., Binz, P. A., Xenarios, I., Eisenacher, M., Mayer, G., Gatto, L., Campos, A., Chalkley, R. J., Kraus, H. J., Albar, J. P., Martinez-Bartolomé, S., Apweiler, R., Omenn, G. S., Martens, L., Jones, A. R. and Hermjakob, H. (2014) *ProteomeXchange provides globally coordinated proteomics data submission and dissemination. Nat Biotechnol*, **32**(3): p. 223-6.
20. Blanc, L., Liu, J., Vidal, M., Chasis, J. A., An, X., and Mohandas, N. (2009) *The water channel aquaporin-1 partitions into exosomes during reticulocyte maturation: implication for the regulation of cell volume. Blood*, **114**(18): p. 3928-34.
21. Géminard, C., De Gassart, A., Blanc, L., and Vidal, M. (2004) *Degradation of AP2 During Reticulocyte Maturation Enhances Binding of Hsc70 and Alix to a Common Site on TfR for Sorting into Exosomes. Traffic*. **5**(3): p. 181-193.
22. Koshino, I., Mohandas, N., and Takakuwa, Y. (2012) *Identification of a novel role for dematin in regulating red cell membrane function by modulating spectrin-actin interaction. J Biol Chem*. **287**(42): p. 35244-50.
23. Manno, S., Takakuwa, Y., and Mohandas, N. (2005) *Modulation of erythrocyte membrane mechanical function by protein 4.1 phosphorylation. J Biol Chem*. **280** (9): p. 7581-7.
24. Ferru, E., Giger, K., Pantaleo, A., Campanella, E., Grey, J., Ritchie, K., Vono, R., Turrini, F., and Low, P. S. (2011) *Regulation of membrane-cytoskeletal interactions by tyrosine phosphorylation of erythrocyte band 3. Blood*, **117**(22): p. 5998-6006.
25. Glodek, A. M., Mirchev, R., Golan, D. E., Khoory, J. A., Burns, J. M., Shevkoplyas, S. S., Nicholson-Weller, A., and Ghiran, I. C. (2010) *Ligation of complement receptor 1 increases erythrocyte membrane deformability. Blood*, **116**(26): p. 6063-71.
26. Horton, E. R., Byron, A., Askari, J. A., Ng, D. H., Millon-Frémillon, A., Robertson, J., Koper, E. J., Paul, N. R., Warwood, S., Knight, D., Humphries,

J. D., and Humphries, M. J. (2015) Definition of a consensus integrin adhesome and its dynamics during adhesion complex assembly and disassembly. *Nat Cell Biol*. **17**(12):1577-87.

27. Konstantinidis, D. G., Pushkaran, S., Johnson, J. F., Cancelas, J. A., Manganaris, S., Harris, C. E., Williams, D. A., Zheng, Y., and Kalfa, T. A. (2012) Signaling and cytoskeletal requirements in erythroblast enucleation. *Blood* **119**, 6118-6127.
28. Wilson, M. C., Trakarnsanga, K., Heesom, K. J., Cogan, N., Green, C., Toye, A. M., Parsons, S. F., Anstee, D. J., and Frayne, J. (2016) Comparison of the Proteome of Adult and Cord Erythroid Cells, and Changes in the Proteome Following Reticulocyte Maturation. *Mol Cell Proteomics* **15**, 1938-1946
29. Carayon, K., Chaoui, K., Ronzier, E., Lazar, I., Bertrand-Michel, J., Roques, V., Balor, S., Terce, F., Lopez, A., Salomé, L., Joly E. (2011) *Proteolipidic composition of exosomes changes during reticulocyte maturation. J Biol Chem*. **286**(39): p. 34426-39.
30. Cao, H., Weller, S., Orth, J. D., Chen, J., Huang, B., Chen, J. L., Stamnes, M., and McNiven, M. A. (2005) *Actin and Arf1-dependent recruitment of a cortactin-dynamin complex to the Golgi regulates post-Golgi transport. Nat Cell Biol*. **7**(5): p. 483-92.
31. Peng, Z., Li, X., Pivkin, I. V., Dao, M., Karniadakis, G. E., and Suresh, S., (2013) Lipid bilayer and cytoskeletal interactions in a red blood cell. *Proc Natl Acad Sci USA*. **13**; 110(33): 13356-61
32. Rochlin, M. W., Dailey, M. E., and Bridgman, P. C. (1999) Polymerizing microtubules activate site-directed F-actin assembly in nerve growth cones. *Mol Biol Cell* **10**, 2309-2327.
33. Ye, F., Lagarrigue, F., and Ginsberg, M. H. (2014) SnapShot: talin and the modular nature of the integrin adhesome. *Cell*. **13**;156 (6):1340-1340.
34. Diez-Silva, M., Dao, M., Han, J., Lim, C. T., and Suresh, S. (2010) Shape and Biomechanical Characteristics of Human Red Blood Cells in Health and Disease. *NIH Public Access*, **35**(5):382-388.
35. Hanspal, M., Yoon, S. H., Yu, H., Hanspal, J. S., Lambert, S., Palek, J., and Prchal, J. T. (1991) Molecular Basis of Spectrin and Ankyrin Deficiencies in

Severe Hereditary Sperocytosis: Evidence Implicating a Primary Defect of Ankyrin. *Blood*, **77**(1):165-73.

36. Mons, B., (1990) *Preferential invasion of malarial merozoites into young red blood cells. Blood Cells*, **16**(2-3): p. 299-312.

37. Clark, M. A., Goheen, M. M., Fulford, A., Prentice, A. M., Elnagheeb, M. A., Patel, J., Fisher, N., Taylor, S. M, Kasthuri, R. S., and Cerami, C. (2014) Host iron status and iron supplementation mediate susceptibility to erythrocytic stage *Plasmodium falciparum*. *Nat Commun*, **5**: p. 4446.

Footnotes

Acknowledgements

TTTC, **AS, RN, RD** and **RC** acknowledge the following grants from Singapore University of Technology & Design to **RC**: SRLS13049, SUTD-ZJU/RES/02/2013, SUTDT12015006. **BR** was funded by Singapore National Medical Research Council (NMRC/CBRG/0047/2013). **BM** was funded by Singapore National Medical Research Council (NMRC/CBRG/0047/2013) and a Young Investigator Grant (BMRC YIG grant no. 13/1/16/YA/009) under the Agency for Science, Technology and Research (A*STAR, Singapore). **LR** was supported by funding from the Singapore Immunology Network (SIgN) and the Horizontal Programme on Infectious Diseases under the Agency for Science, Technology and Research (A*STAR, Singapore). **NKV** acknowledges Lee Kong Chian School of Medicine, Nanyang Technological University Start-Up Grant and the Ministry of Education Singapore AcRF Tier 1 grant (2014-T1-001-141). Mohit Arora's technical assistance in initial AFM imaging attempts is greatly acknowledged. **RC** acknowledges the infrastructure support from SUTD-MIT International Design Centre (IDC) and Singapore-MIT Alliance for Research & Technology Centre (SMART), supported by the National Research Foundation. RC thanks Prof. Chwee Teck Lim (NUS), Prof. Ming Dao (MIT) and Prof. Peter Preiser (NTU) for various discussions.

Author Contributions

CTTT: Involved in study design, performed research, analysed data & assisted in manuscript preparation; **AS**: Involved in study design, performed research, analysed data & assisted in manuscript preparation; **BM**: provided reagents & performed research; **RS**: provided reagents & performed research; **JEP**: performed research & analysed data; **RN**: performed research & assisted in manuscript preparation; **RD**: performed research & assisted in manuscript preparation; **STO**: performed microscopy analysis and assisted in manuscript preparation; **NKV**: Involved in the design of microscopy experiments, analysed microscopy data and assisted in manuscript preparation; JKC: provided reagents, verified results & assisted in manuscript preparation**;** **FN**: provided reagents & verified results; **LR**: provided

reagents, verified results & assisted in manuscript preparation; **SSK:** analysed data, verified results & assisted in manuscript preparation; **BMR**: Involved in study design, verified results & assisted in manuscript preparation; **RC**: Designed the study, analysed data, coordinated research, verified results and wrote the paper.

Figure Legends

Scheme 1: Scheme demonstrating the overall strategy adopted for enrichment of $CD71^+$ and $CD71^-$ red blood cell populations from cord blood, sample fractionation and mass spectrometry.

Figure. 1: Isolation and characterization of $CD71^+$ and $CD71^-$ red blood cells. (A) Reticulocytes that are $CD71^+$ (Upper Panel) and mature red cells $CD71^-$(Lower Panel) were purified from cord blood collected from 5 individual donors, by a magnetic selection procedure using anti-CD71-conjugated microbeads and purity validated by flow cytometry using Thiazole orange staining, **(B)** sub-vital staining, **(C)** Immunofluorescence staining using anti-CD71 antibody and **(D)** Western blotting. **(E)** Representative SDS-PAGE profile that corresponds to $CD71^+$ and $CD71^-$ red blood cells fractionated into membrane and luminal components. SDS-PAGE pattern demonstrates robust fractionation of membranes from the luminal fraction, as represented by enrichment of spectrins (~ 250kDa) and band 3 (~100kDa) and reduction in haemoglobin (~15kDa), indicated by arrowheads**.**

Figure. 2: Analyses of the quantitative mass spectrometry results (A) Ingenuity analyses revealed pathways that had undergone significant alterations during reticulocyte maturation. Red colour indicates up-regulation (abundance) and the green, down-regulation (reduction or loss) during maturation of $CD71^+$ reticulocytes. **(B)** Gene Ontology-based distribution of abundant proteins from $CD71^+$ reticulocyte membrane fraction, according to biological processes they are associated with. Proteins enriched in $CD71^+$ reticulocytes were mostly involved in metabolic/translational processes **(C)** Proteins that were abundant in immature reticulocytes are presented according to sub-cellular localization.

Figure. 3: Gene Ontology-based distribution of luminal proteins that are abundant in $CD71^+$ reticulocytes, according to **(A)** biological processes they are involved in and **(B)** sub-cellular localization. Proteins enriched in $CD71^+$ reticulocytes were mostly involved in synthetic/translational processes.

Figure. 4: Gene Ontology-based distribution of luminal proteins that had undergone reduction during maturation of $CD71^+$ reticulocytes according to **(A)** biological processes they are involved in and **(B)** sub-cellular localization.

Figure. 5: Major changes observed to the red cell structural components during reticulocyte maturation **(A)** Selected surface exposed membrane proteins identified by mass spectrometry is presented as a function of relative abundance (Log_2(Fold change)). High abundance of CD71 in immature reticulocytes was observed while most other surface proteins were detected in similar abundance from both stages of red cells **(B)** Abundance of cytoskeletal proteins such as spectrins, ankyrin and band 4.1 remained comparable between $CD71^+$ and $CD71^-$ red cells, while talin and ß-tubulin were present in $CD71^+$ cells in abundance. **(C)**Western blotting confirmed the enrichment of Talin-1/2 and ß-tubulin in immature reticulocytes.

Figure. 6: Validation of the presence of ß-tubulin and talin-1 on $CD71^+$ reticulocytes and their loss upon maturation. Presence of ß-tubulin **(A,** green**)** and talin-1 **(B,** green**)** in $CD71^+$ reticulocytes was confirmed by immunofluorescence confocal microscopy; $CD71^-$ normocytes showed no signal for these two proteins. Cells were counter-stained with Cell Mask™ (red) to visualize cellular morphologies and membrane structures.

Figure. 7: Membrane biomechanical properties and cytoskeletal deformations upon reticulocyte maturation. (A) $CD71^+$ retciculocytes were allowed to mature *ex vivo*, and membrane biomechanical properties were measured using micropipette aspiration method at various stages of maturation. Freshly isolated $CD71^+$ reticulocytes were rigid (with an average shear modulus 18.9 pN/µm**)** and lobular, while they became highly deformable upon maturation over 40 h (average shear modulus 6.4 pN/µm. (B) AFM-imaging of cytosolic side- exposed cells revealed significant nano-structural differences between immature reticulocytes and normocytes **(C)** shrinkage of spectrin filaments during reticulocyte maturation was estimated from skeletonized images obtained through AFM (Scale bar: 100 nm).

While the average length of spectrin filament was 48nm in $CD71^+$ reticulocytres, it was reduced to 41nm in $CD71^-$ cells, in agreement with prior reports.

Supplemental Dataset 1: Mass spectrometry data (For review purpose only)
Project Name: Reticulocytes vs mature red blood cell
Project accession: PXD003851

Reviewer account details:

Username: mailto:reviewer25260@ebi.ac.uk
Password: wwtcEhDi

Supplement Dataset 2: All peptides

Supplemental Figure Legends

Supplemental Figure S1: (A) Sequence coverage, (B) Fold difference and (C) mass spectra for beta-tubulin.

Supplemental Figure S2: (A) Sequence coverage, (B) Fold difference and (C) mass spectra for Talin1/2.

Supplemental Figure S3: Super-resolution confocal images of Band 3 immunofluorescenece staining on $CD71^+$ reticlucytes (upper panel) and $CD71^-$ red blood cells (lower panel).

Scheme. 1

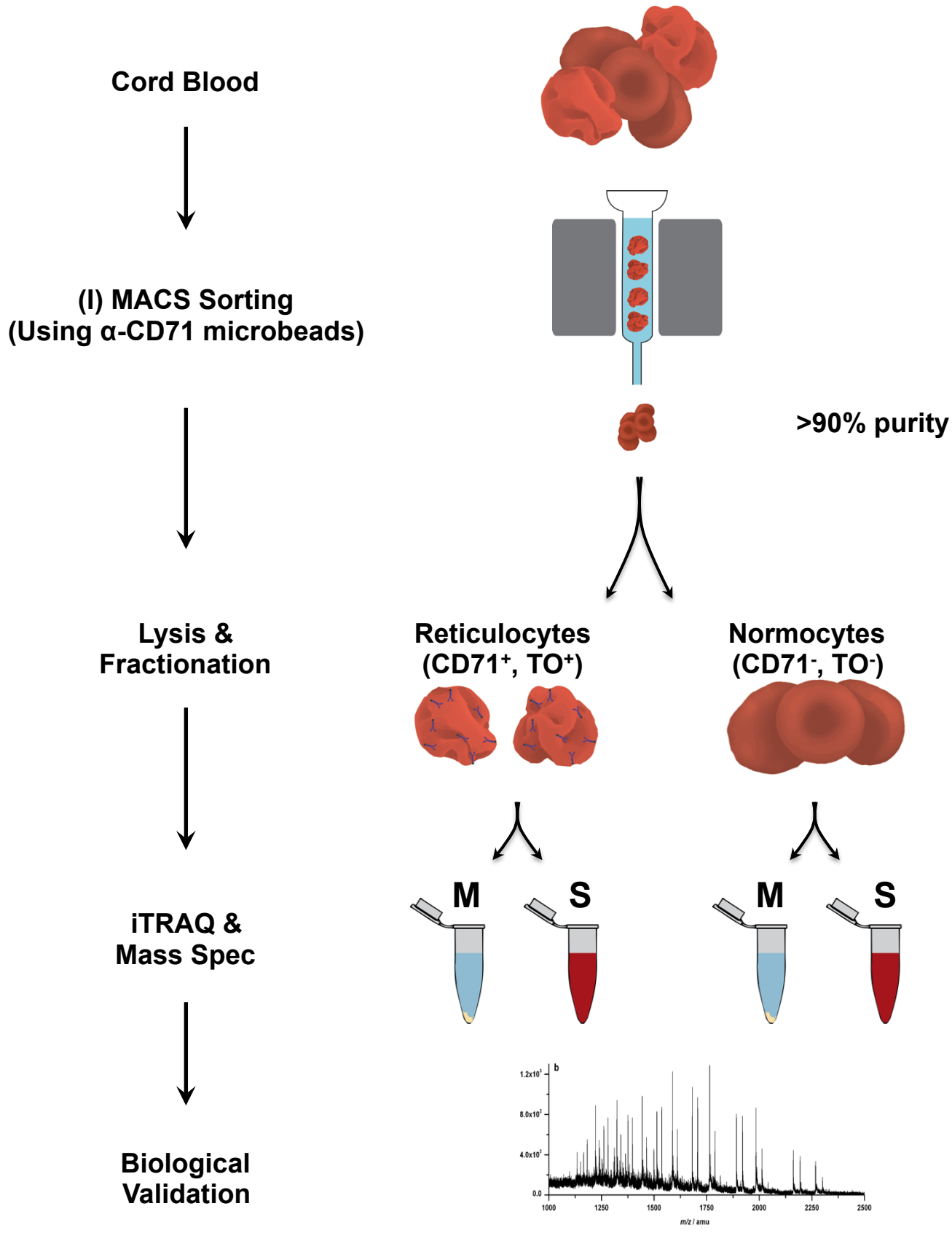
Cord Blood
(I) MACS Sorting
(Using α-CD71 microbeads)
>90% purity
Lysis &
Fractionation
Reticulocytes
(CD71+, TO+)
Normocytes
(CD71-, TO-)
iTRAQ &
Mass Spec
M
S
M
S
Biological
Validation
b
1.2x10³
8.0x10²
4.0x10²
0.0
1000
1250
1500
1750
2000
2250
2500
m/z / amu

Figure. 1

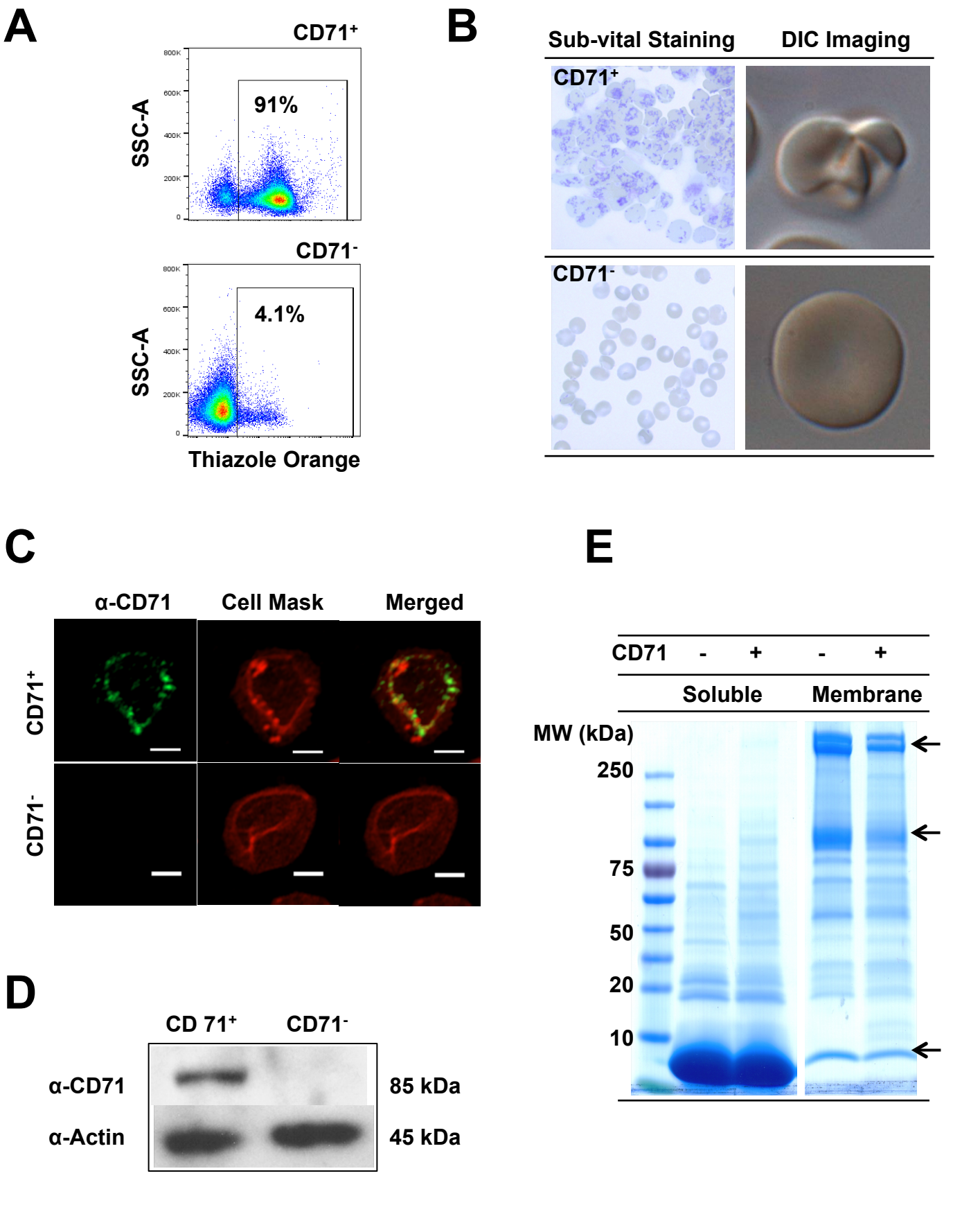
A
CD71+
91%
SSC-A
CD71-
4.1%
SSC-A
Thiazole Orange
B
Sub-vital Staining
DIC Imaging
CD71+
CD71-
C
α-CD71
Cell Mask
Merged
CD71+
CD71-
D
CD 71+
CD71-
α-CD71
α-Actin
85 kDa
45 kDa
E
CD71 - + - +
Soluble
Membrane
MW (kDa)
250
75
50
20
10

Figure. 2

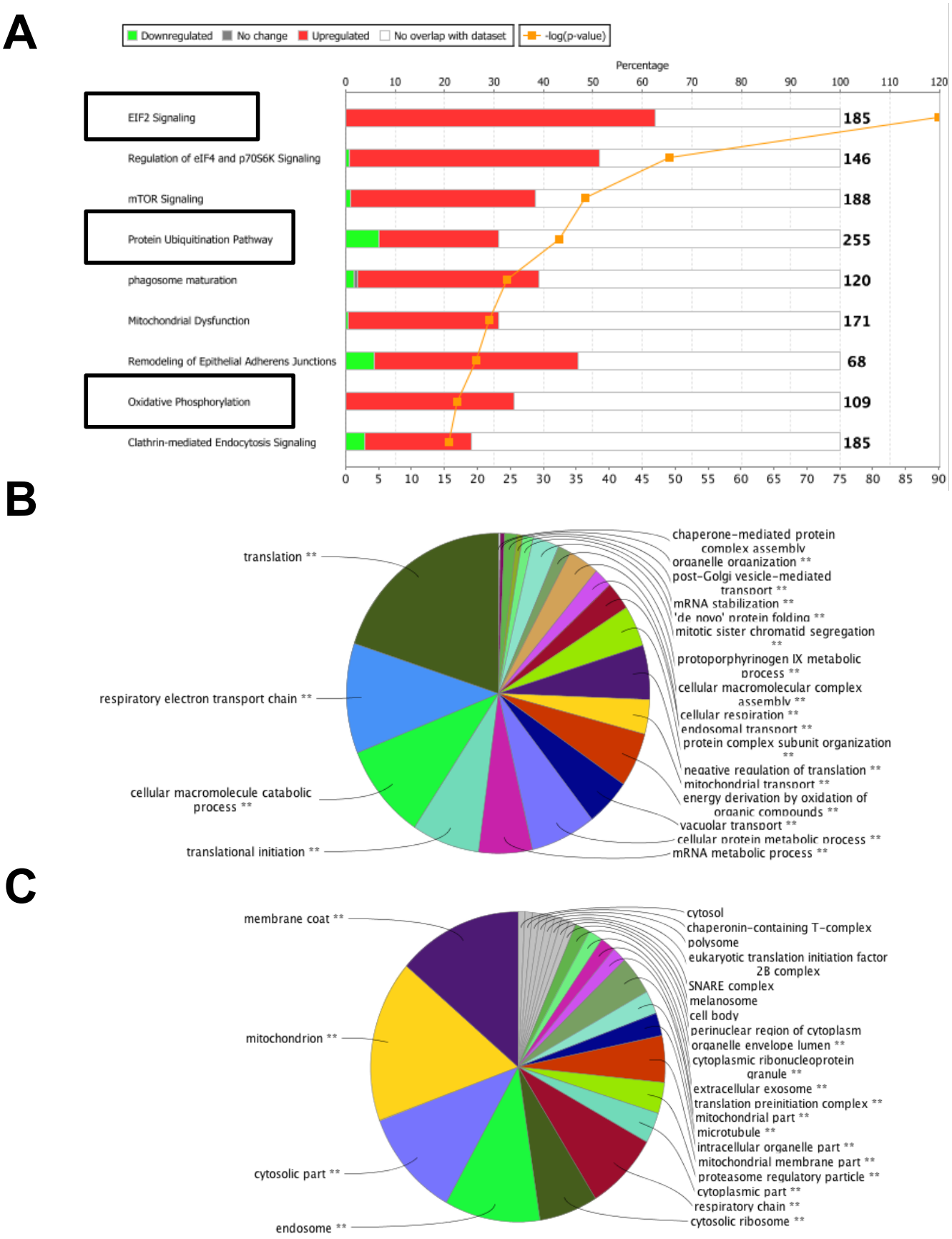
A
Downregulated
No change
Upregulated
No overlap with dataset
-log(p-value)
Percentage
EIF2 Signaling
Regulation of eIF4 and p70S6K Signaling
mTOR Signaling
Protein Ubiquitination Pathway
phagosome maturation
Mitochondrial Dysfunction
Remodeling of Epithelial Adherens Junctions
Oxidative Phosphorylation
Clathrin-mediated Endocytosis Signaling
185
146
188
255
120
171
68
109
185
B
translation **
respiratory electron transport chain **
cellular macromolecule catabolic process **
translational initiation **
chaperone-mediated protein complex assembly
organelle organization **
post-Golgi vesicle-mediated transport **
mRNA stabilization **
'de novo' protein folding **
mitotic sister chromatid segregation **
protoporphyrinogen IX metabolic process **
cellular macromolecular complex assembly **
cellular respiration **
endosomal transport **
protein complex subunit organization **
negative regulation of translation **
mitochondrial transport **
energy derivation by oxidation of organic compounds **
vacuolar transport **
cellular protein metabolic process **
mRNA metabolic process **
C
membrane coat **
mitochondrion **
cytosolic part **
endosome **
cytosol
chaperonin-containing T-complex
polysome
eukaryotic translation initiation factor 2B complex
SNARE complex
melanosome
cell body
perinuclear region of cytoplasm
organelle envelope lumen **
cytoplasmic ribonucleoprotein granule **
extracellular exosome **
translation preinitiation complex **
mitochondrial part **
microtubule **
intracellular organelle part **
mitochondrial membrane part **
proteasome regulatory particle **
cytoplasmic part **
respiratory chain **
cytosolic ribosome **

Figure. 3

A

Biological Process

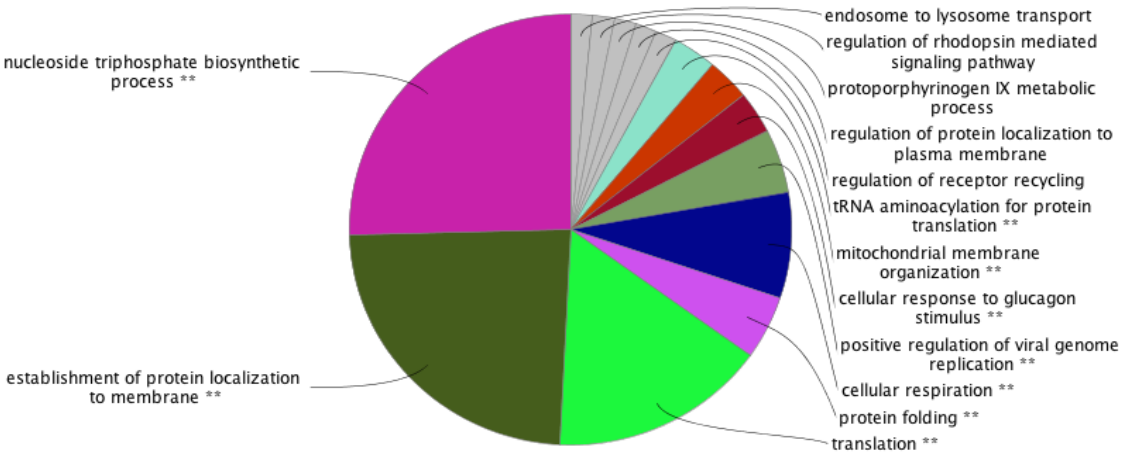

B

Subcellular localization

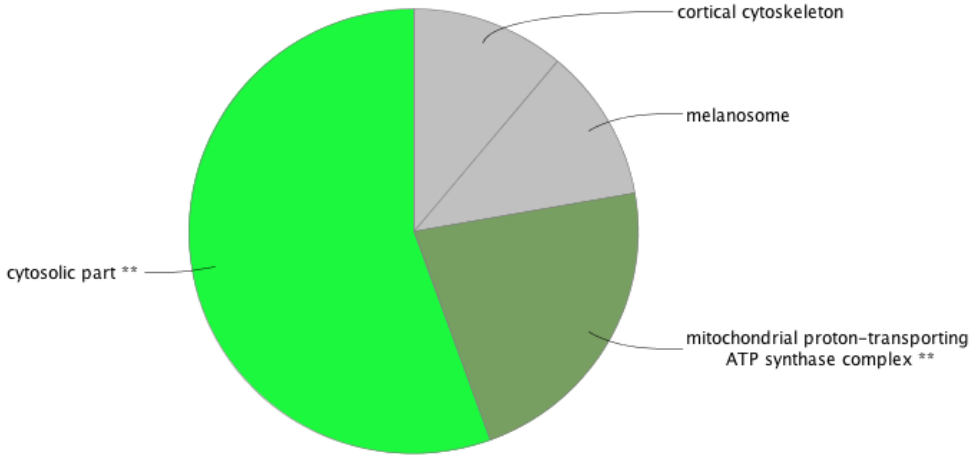

Figure. 4

A

Biological Process

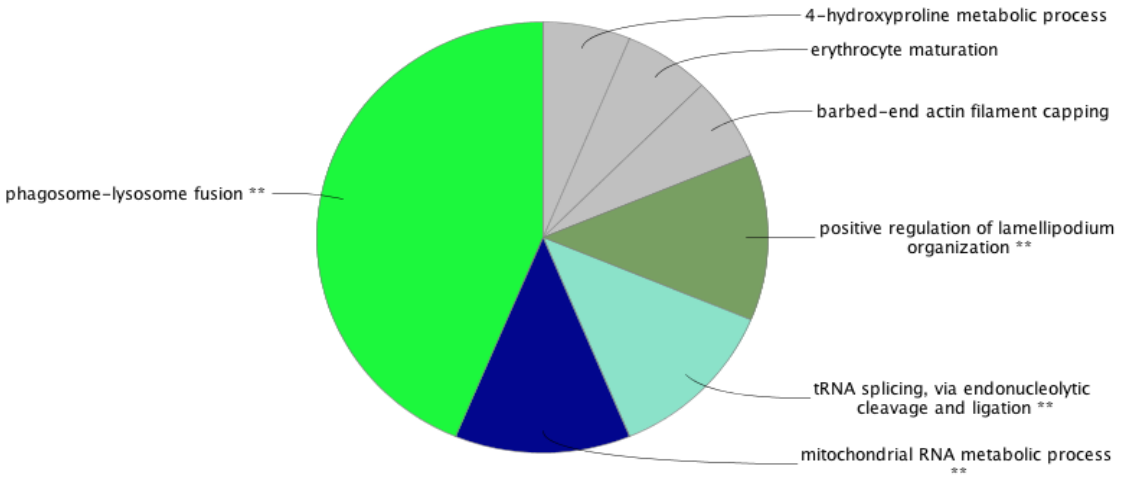

B

Subcellular localization

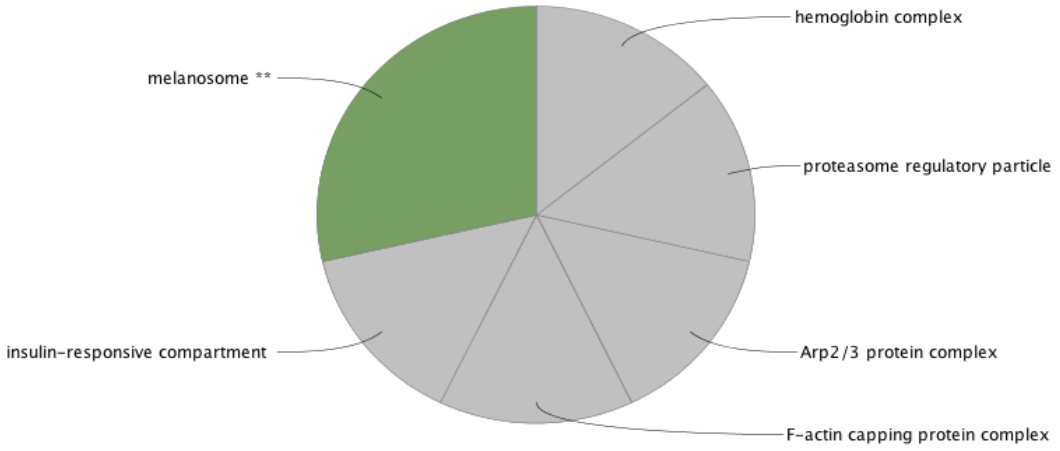

Figure. 5

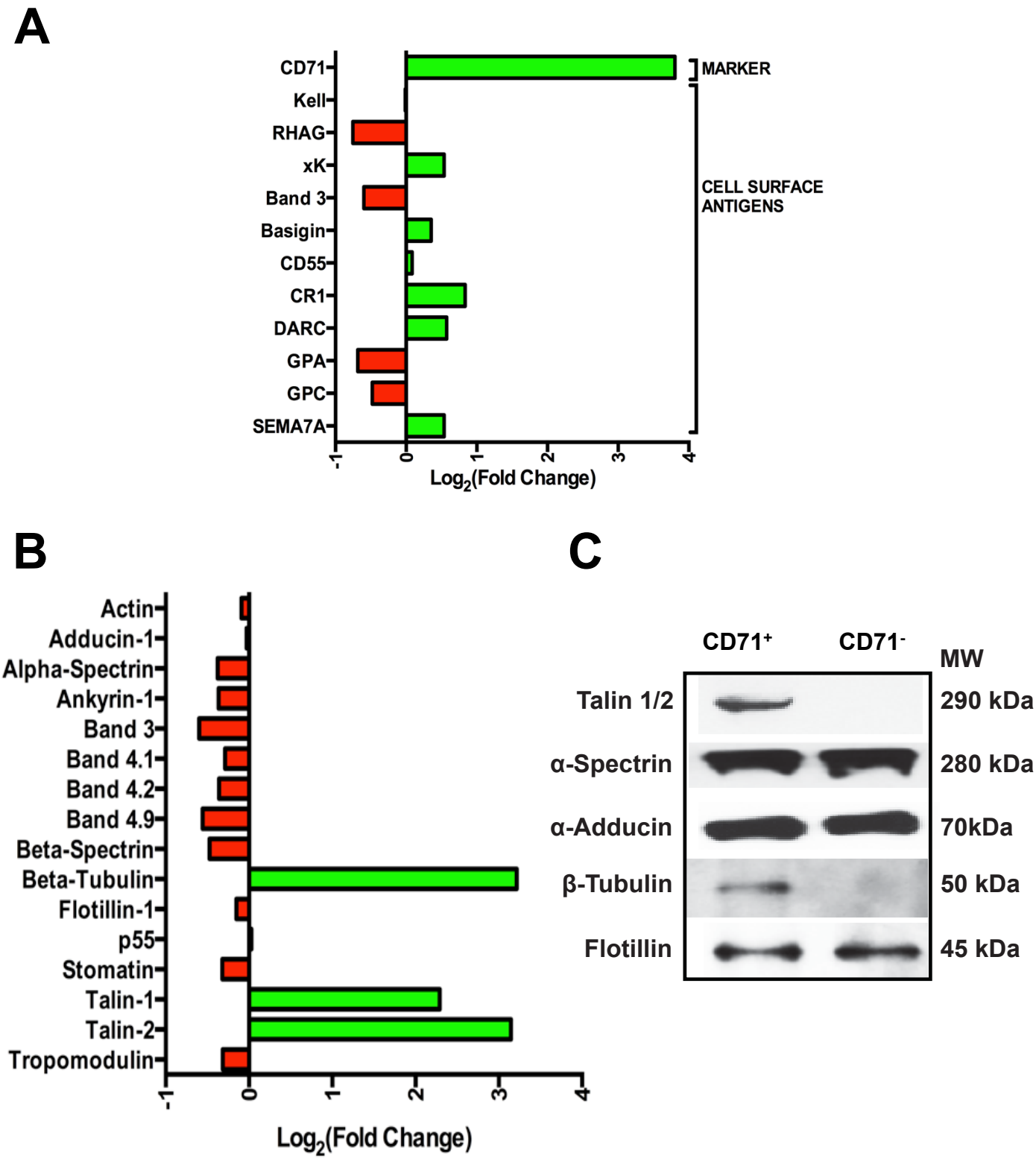
A
CD71
Kell
RHAG
xK
Band 3
Basigin
CD55
CR1
DARC
GPA
GPC
SEMA7A
MARKER
CELL SURFACE ANTIGENS
-1
0
1
2
3
4
Log2(Fold Change)
B
Actin
Adducin-1
Alpha-Spectrin
Ankyrin-1
Band 3
Band 4.1
Band 4.2
Band 4.9
Beta-Spectrin
Beta-Tubulin
Flotillin-1
p55
Stomatin
Talin-1
Talin-2
Tropomodulin
-1
0
1
2
3
4
Log2(Fold Change)
C
CD71+
CD71-
MW
Talin 1/2
290 kDa
α-Spectrin
280 kDa
α-Adducin
70kDa
β-Tubulin
50 kDa
Flotillin
45 kDa

Figure. 6

A

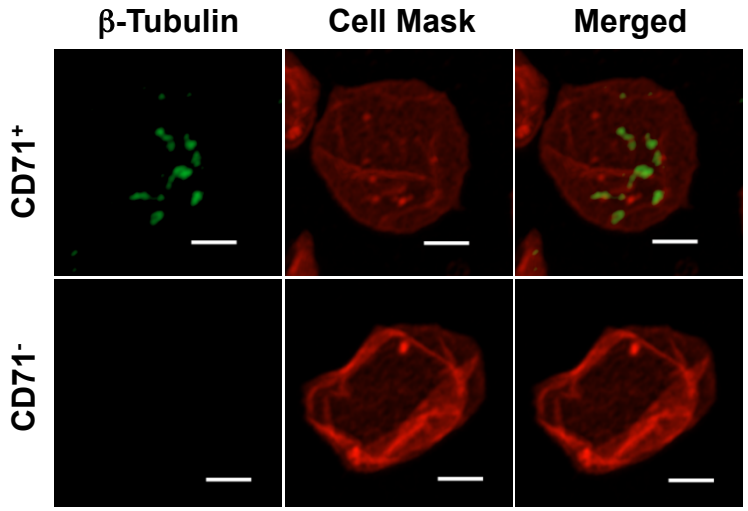
β-Tubulin
Cell Mask
Merged
CD71+
CD71-

B

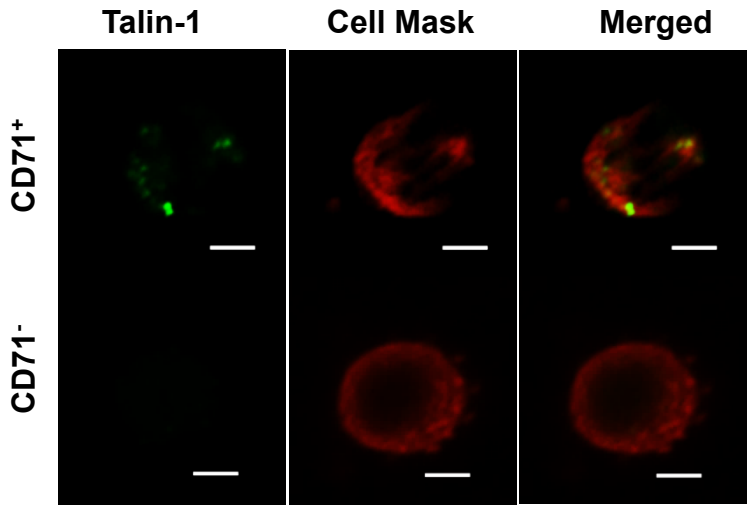
Talin-1
Cell Mask
Merged
CD71+
CD71-

Figure. 7

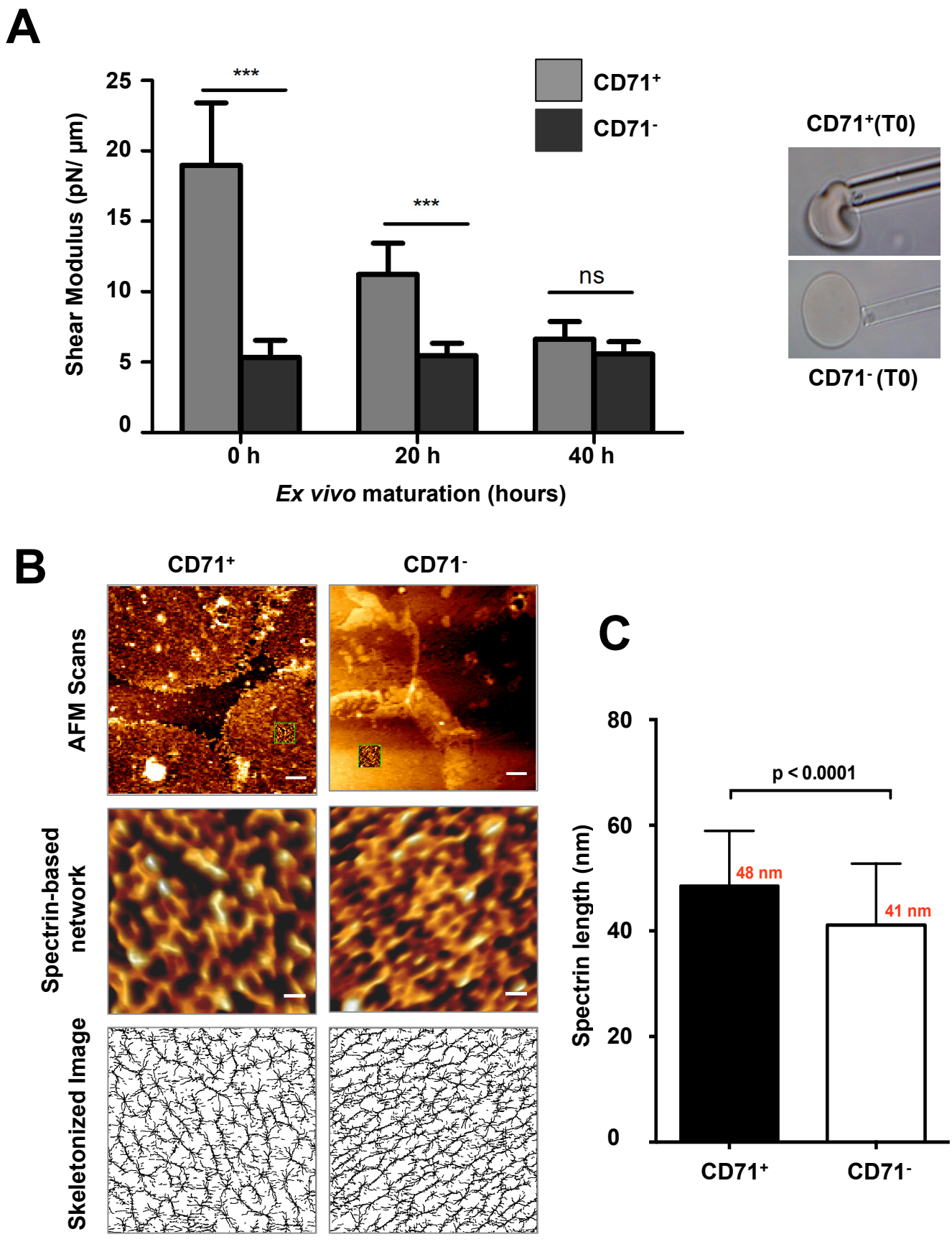
A
Shear Modulus (pN/ µm)
25
20
15
10
5
0
***
***
ns
CD71+
CD71-
0 h
20 h
40 h
Ex vivo maturation (hours)
CD71+(T0)
CD71- (T0)
B
CD71+
CD71-
AFM Scans
Spectrin-based network
Skeletonized Image
C
Spectrin length (nm)
80
60
40
20
0
p < 0.0001
48 nm
41 nm
CD71+
CD71-

Supplemental Figure. S1

A

TBB4B_HUMAN (100%) 49,830.7 Da
Tubulin beta-4B chain OS=Homo sapiens GN=TUBB4B PE=1 SV=1

M	R	E	I	V	H	L	Q	A	G	Q	C	G	N	Q	I	G	A	K	F	W	E	V	I	S	D	E	H	G	I	D	P	T	G	T	Y	H	G	D	S	D	L	Q	L	E	R	I	N	V	Y	Y	N	E	A	T	G	G	K	Y	V
P	R	A	V	L	V	D	L	E	P	G	T	M	D	S	V	R	S	G	P	F	G	Q	I	F	R	P	D	N	F	V	F	G	Q	S	G	A	G	N	N	W	A	K	G	H	Y	T	E	G	A	E	L	V	D	S	V	L	D	V	V
R	K	E	A	E	S	C	D	C	L	Q	G	F	Q	L	T	H	S	L	G	G	G	T	G	S	G	M	G	T	L	L	I	S	K	I	R	E	E	Y	P	D	R	I	M	N	T	F	S	V	V	P	S	P	K	V	S	D	T	V	V
E	P	Y	N	A	T	L	S	V	H	Q	L	V	E	N	T	D	E	T	Y	C	I	D	N	E	A	L	Y	D	I	C	F	R	T	L	K	L	T	T	P	T	Y	G	D	L	N	H	L	V	S	A	T	M	S	G	V	T	T	C	L
R	F	P	G	Q	L	N	A	D	L	R	K	L	A	V	N	M	V	P	F	P	R	L	H	F	F	M	P	G	F	A	P	L	T	S	R	G	S	Q	Q	Y	R	A	L	T	V	P	E	L	T	Q	Q	M	F	D	A	K	N	M	M
A	A	C	D	P	R	H	G	R	Y	L	T	V	A	A	V	F	R	G	R	M	S	M	K	E	V	D	E	Q	M	L	N	V	Q	N	K	N	S	S	Y	F	V	E	W	I	P	N	N	V	K	T	A	V	C	D	I	P	P	R	G
L	K	M	S	A	T	F	I	G	N	S	T	A	I	Q	E	L	F	K	R	I	S	E	Q	F	T	A	M	F	R	R	K	A	F	L	H	W	Y	T	G	E	G	M	D	E	M	E	F	T	E	A	E	S	N	M	N	D	L	V	S
E	Y	Q	Q	Y	Q	D	A	T	A	E	E	E	G	E	F	E	E	E	A	E	E	E	V	A																																			

B

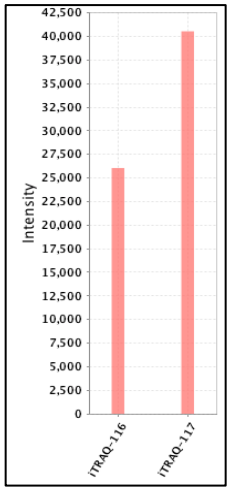

C

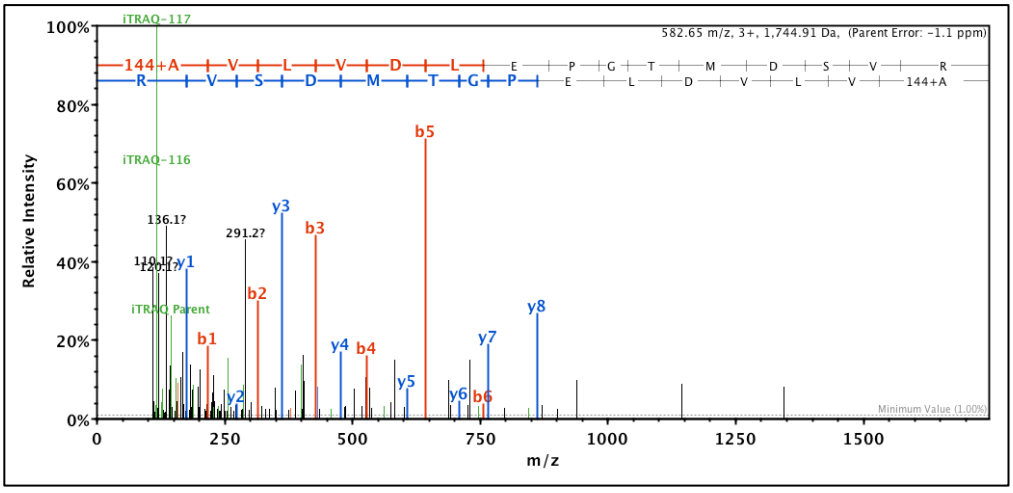

Supplemental Figure. S2

A

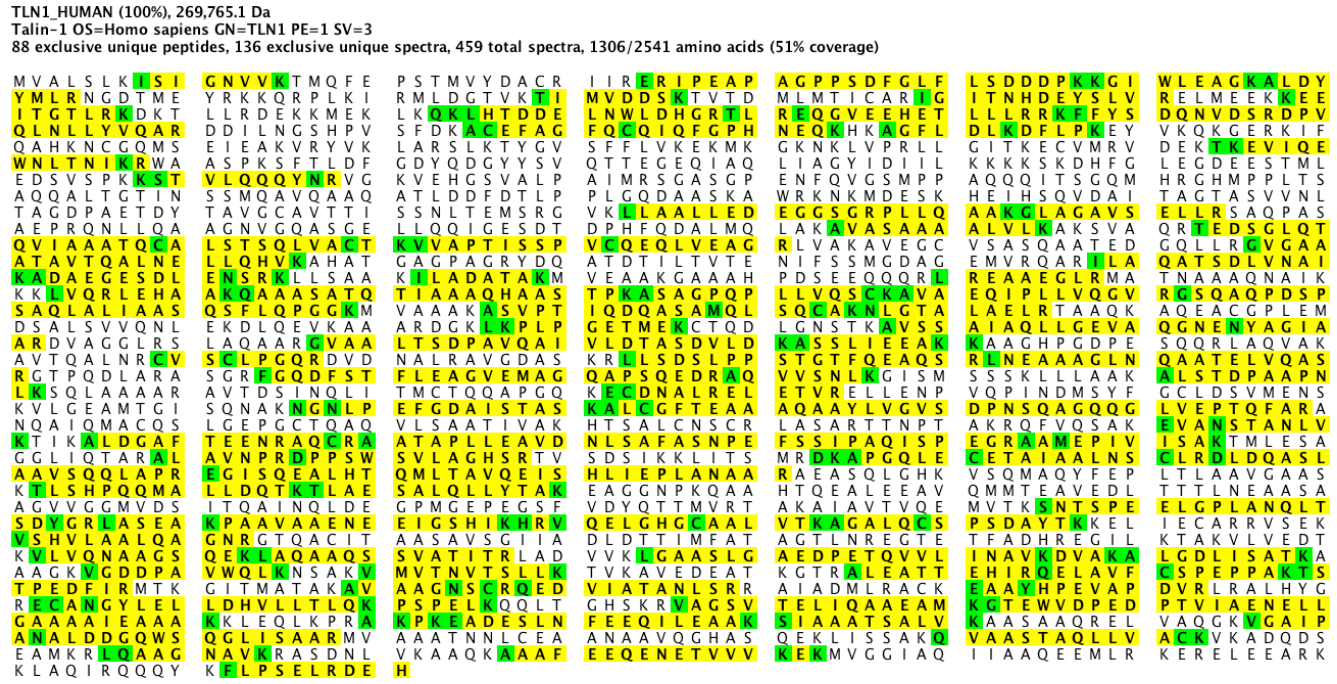

B

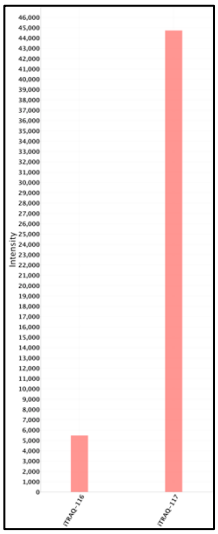

C

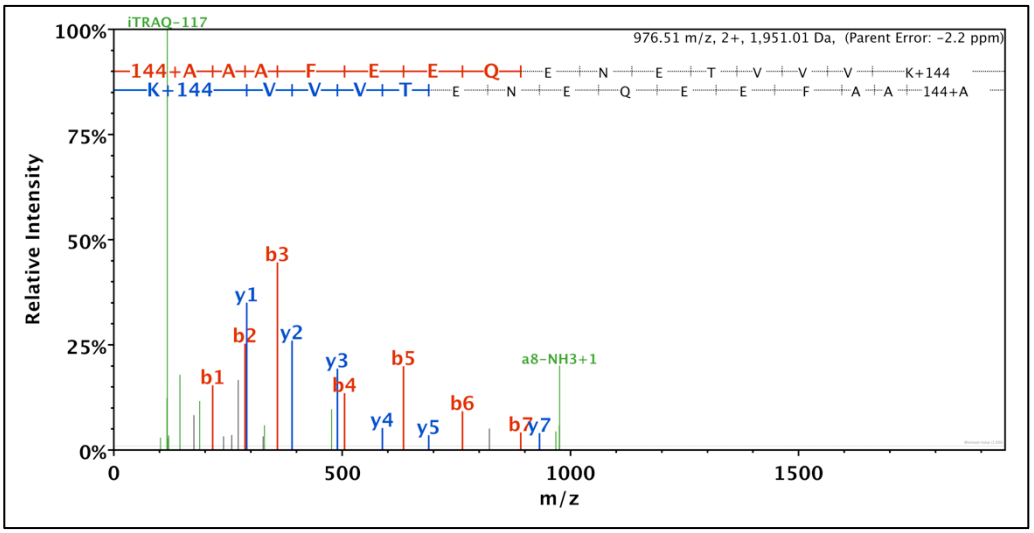

Supplemental Figure. S3

A